



# Controlled Scalable Synthesis of Uniform, High-Quality Monolayer and Few-layer MoS<sub>2</sub> Films

Yifei Yu<sup>1</sup>, Chun Li<sup>1</sup>, Yi Liu<sup>3</sup>, Liqin Su<sup>4</sup>, Yong Zhang<sup>4</sup> & Linyou Cao<sup>1,2</sup>

<sup>1</sup>Department of Materials Science and Engineering, North Carolina State University, Raleigh NC 27695, <sup>2</sup>Department of Physics, North Carolina State University, Raleigh NC 27695, <sup>3</sup>Analytical Instrumentation Facility, North Carolina State University, Raleigh NC 27695, <sup>4</sup>Department of Electrical and Computer Engineering, The University of North Carolina at Charlotte, Charlotte, NC 28223.

Received  
5 April 2013

Accepted  
7 May 2013

Published  
21 May 2013

Correspondence and  
requests for materials  
should be addressed to  
L.C. (lcao2@ncsu.edu)

Two dimensional (2D) materials with a monolayer of atoms represent an ultimate control of material dimension in the vertical direction. Molybdenum sulfide (MoS<sub>2</sub>) monolayers, with a direct bandgap of 1.8 eV, offer an unprecedented prospect of miniaturizing semiconductor science and technology down to a truly atomic scale. Recent studies have indeed demonstrated the promise of 2D MoS<sub>2</sub> in fields including field effect transistors, low power switches, optoelectronics, and spintronics. However, device development with 2D MoS<sub>2</sub> has been delayed by the lack of capabilities to produce large-area, uniform, and high-quality MoS<sub>2</sub> monolayers. Here we present a self-limiting approach that can grow high quality monolayer and few-layer MoS<sub>2</sub> films over an area of centimeters with unprecedented uniformity and controllability. This approach is compatible with the standard fabrication process in semiconductor industry. It paves the way for the development of practical devices with 2D MoS<sub>2</sub> and opens up new avenues for fundamental research.

The significance of 2D materials has been manifested by a plethora of fascinating functionality demonstrated in graphene, a monolayer material of carbon atoms<sup>1–4</sup>. In contrast to graphene, which is a semi-metal with no bandgap by nature, MoS<sub>2</sub> monolayers offer an attractive semiconductor option due to a direct bandgap of 1.8 eV<sup>5,6</sup>. This non-trivial bandgap makes MoS<sub>2</sub> monolayers a better candidate than graphene to revolutionize many electronic and photonic devices that are currently dominated by traditional group IV or III–V semiconductor materials<sup>7–23</sup>. Considerable efforts have been dedicated to achieve scalable synthesis of high quality MoS<sub>2</sub> monolayers that is necessary for the development of practical devices. These include sulfurization of MoO<sub>3</sub> or Mo layers pre-deposited on substrates, or thermolysis of Mo compound (NH<sub>4</sub>)<sub>2</sub>MoS<sub>4</sub><sup>24–31</sup>. However, none of the existing processes provides the capability to exclusively produce uniform MoS<sub>2</sub> monolayers over a large area up to centimeters. Additionally, none of these processes is able to precisely control the layer number of MoS<sub>2</sub> films. For instance, MoS<sub>2</sub> monolayers resulted from these processes always co-exist with by-products of thicker layers. As the properties of MoS<sub>2</sub> materials strongly depend on the layer number, this unsatisfactory uniformity and controllability poses a formidable challenge for the improvement of device performance. Here we present a new, self-limiting chemical vapor deposition (CVD) approach that can exclusively grow high-quality monolayer or few-layer MoS<sub>2</sub> films over an area of centimeters on various substrates such as silicon oxide, sapphire, and graphite. The layer number of the MoS<sub>2</sub> films can be precisely controlled as 1, 2, 3, and beyond. The synthesized film shows unprecedented uniformity with no other layers found by thorough characterizations. It exhibits optical and electrical quality comparable to the MoS<sub>2</sub> exfoliated from bulk materials, and can be transferred to other arbitrary substrates.

## Results

We grew MoS<sub>2</sub> films at high temperatures (> 800°C) using MoCl<sub>5</sub> and sulfur as precursor materials (we found the quality of resulting thin films worse at lower growth temperatures). The precursor materials can react at elevated temperatures to produce MoS<sub>2</sub> species, which may subsequently precipitate onto receiving substrates to yield MoS<sub>2</sub> films (Fig. S1). The layer number of the resulting MoS<sub>2</sub> films can be very precisely controlled by controlling the amount of MoCl<sub>5</sub> used in experiments or the total pressure in the synthetic setup (details see Studies of growth mechanism in the Supplementary Information). We have successfully grown monolayer or few-layer MoS<sub>2</sub> films on various substrates including silicon oxide, sapphire, and graphite. Fig. 1 a–b show optical images of the MoS<sub>2</sub>

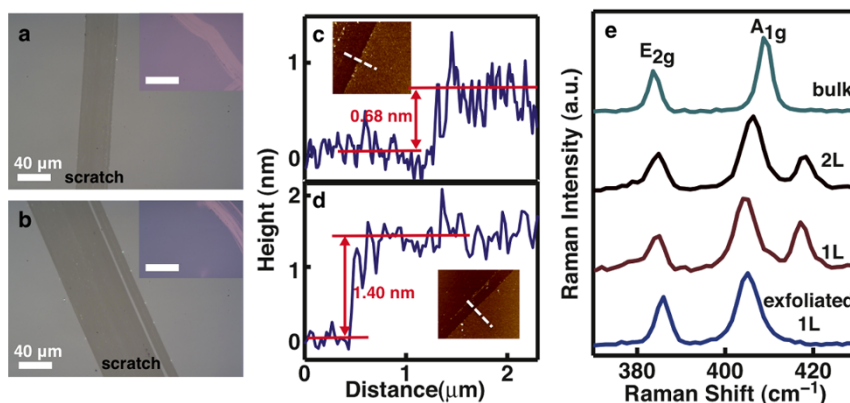


**Figure 1 | Controlled synthesis of MoS<sub>2</sub> monolayer and bilayer films.** (a) and (b), Optical images of the MoS<sub>2</sub> monolayer and bilayer films grown on sapphire substrates, respectively. The insets are optical images of the MoS<sub>2</sub> monolayer and bilayer films grown on SiO<sub>2</sub>/Si substrates. The scale bars in the insets are 80 μm. (c) and (d), AFM height profiles for typical MoS<sub>2</sub> monolayer and bilayer films grown on sapphire, respectively. The insets show the AFM images from which the height profiles are extracted. A larger version of the AFM images is given in Fig.S3 of the Supplementary Information. (e), Raman spectra of the MoS<sub>2</sub> monolayer (1 L) and bilayer (2 L) films grown on sapphire. Also given are the Raman spectra of exfoliated MoS<sub>2</sub> monolayer and bulk MoS<sub>2</sub> dispersed on SiO<sub>2</sub>/Si substrates. The two characteristic Raman modes are labeled. The peak at 418 cm<sup>-1</sup> is from the sapphire substrate.

monolayer and bilayer films grown on sapphire substrates. The optical images of MoS<sub>2</sub> monolayer and bilayer films grown on silicon substrates with 280 nm thick silicon oxide (SiO<sub>2</sub>/Si) are also given as insets. Scratches were intentionally introduced to show the color contrast between the thin film and the substrate (no MoS<sub>2</sub> film exists in the scratched area). We confirm the chemical composition of the thin films is MoS<sub>2</sub> using x-ray photoelectron spectroscopy (XPS) characterizations (Fig. S2). From the optical images, we can find that the thin films are continuous and uniform over a large area. We can also find that the color contrasts of MoS<sub>2</sub> monolayer and bilayer films bear little difference on sapphire but are substantially different on SiO<sub>2</sub>/Si, the monolayer showing pink color while the bilayer more bluish. This substantial difference in color contrast may provide a facile approach to determine the thickness of 2D MoS<sub>2</sub> materials.

We characterized the synthesized thin films using atomic force microscope (AFM) and Raman spectroscopy. The thickness of the synthesized MoS<sub>2</sub> monolayers and bilayers are shown 0.68 nm and 1.40 nm (Fig. 1c–d), in consistence with exfoliated MoS<sub>2</sub> (Fig. S3–S5). Fig. 1e shows the Raman spectra collected from the as-grown MoS<sub>2</sub> thin films on sapphire with different layer numbers (the Raman spectra for the MoS<sub>2</sub> films grown on SiO<sub>2</sub>/Si is given in Fig. S6). The Raman spectra of exfoliated MoS<sub>2</sub> monolayers and bulk MoS<sub>2</sub> materials are also given in Fig. 1e as references. Two characteristic Raman modes can be found in the spectra, the A<sub>1g</sub> mode associated with the out-of-plane vibration of sulfur atoms and the E<sub>2g</sub> mode related with the in-plane vibration of Mo and sulfur atoms<sup>32–34</sup>. The full width at half maximum (FWHM) of the E<sub>2g</sub> peak may be used as an indicator for crystalline quality. The E<sub>2g</sub> FWHM of the synthesized MoS<sub>2</sub> monolayer is 4.2 cm<sup>-1</sup>, close to that of the exfoliated monolayer, 3.7 cm<sup>-1</sup>. This suggests a good crystalline quality in the synthesized film. Additionally, the frequency difference ( $\Delta k$ ) between the E<sub>2g</sub> and A<sub>1g</sub> modes has been known closely related with the layer number, and can be used to determine the thickness of MoS<sub>2</sub> materials<sup>32–34</sup>. We can find that the frequency difference  $\Delta k$  of the synthesized thin film increases with the thickness (Fig. 1e), consistent with what were observed on exfoliated MoS<sub>2</sub><sup>32–34</sup>. A systematic correlation between the value of  $\Delta k$  and the layer number of the synthesized film is given in Table S1 of the Supplementary Information. The  $\Delta k$  of the synthesized film is generally larger than that of exfoliated MoS<sub>2</sub>. For example, the  $\Delta k$  of the synthesized monolayer is found around 20.4 cm<sup>-1</sup>, different from that of the exfoliated monolayer, 19.4 cm<sup>-1</sup>. This could be related with certain crystalline imperfection, for example, smaller crystalline grains in the synthesized thin film.

Other groups also observed a larger  $\Delta k$  in synthesized MoS<sub>2</sub> materials than exfoliated counterparts<sup>26</sup>.

The synthesized MoS<sub>2</sub> thin films show unprecedented uniformity. We can find the as-grown MoS<sub>2</sub> thin films continuous and uniform cross an area of centimeters under optical microscope or by eyes, as illustrated by Fig. 1a and 2a. To more quantitatively assess the uniformity over a large area, we divided the monolayer MoS<sub>2</sub> film grown on a typical sapphire substrate in size of 1 cm × 3 cm into eight areas (Fig. 2b inset). We measured numerous Raman spectra at each of the areas, and plotted the representative results in Fig. 2b. We can find that the peak positions of the E<sub>2g</sub> and A<sub>1g</sub> modes remain identical in all the spectra. The profile of the Raman peaks, such as the FWHM, shows negligible difference. This indicates that the synthesized thin film is indeed a homogeneous monolayer with similar crystalline quality across the entire substrate. We also performed Raman mapping over an area of 10 μm × 10 μm in the as-grown monolayer film, and plotted the measured frequency difference  $\Delta k$  in a 2D image (Fig. 2c). All the  $\Delta k$  are found in a range of 20.3 – 20.7 cm<sup>-1</sup>, confirming the film a homogeneous monolayer. To further confirm the uniformity, we performed multiple AFM measurements at different areas on the film, and found similar thickness and surface topology in all the AFM images (Fig. S8). A typical AFM measurement (5 μm × 5 μm) is given in Fig. 2d. It shows a continuous and smooth surface (roughness < 0.2 nm) with no step and void observed. Similar uniformity can also be found at the synthesized bilayer MoS<sub>2</sub> film (Fig. S9–S10). We should note that the size of the synthesized thin film (1 cm × 3 cm) is limited by the size and temperature uniformity of our current synthetic setup. We believe that by optimizing the synthetic setup we can produce wafer-scale MoS<sub>2</sub> monolayer or few-layer films.

The synthesized MoS<sub>2</sub> films exhibit a very good crystalline quality as indicated by the Raman measurements (Fig. 1e and 2b). To further elucidate the crystalline structure, we characterized the thin film using aberration-corrected scanning transmission electron microscope (STEM). To do that, we transferred the synthesized film to TEM grids following a process reported in references<sup>25</sup>. The synthesized film is found as polycrystalline with crystalline grains varying from tens to hundreds of nanometers as indicated by selected area electron diffraction patterns (Fig. S11). We used high angle annular dark field (HAADF) imaging to investigate the atomic arrangement in the synthesized MoS<sub>2</sub> monolayer and bilayer films. The monolayer and the bilayer can be identified from the folding edge of the transferred thin film (Fig. 3a inset). Fig. 3a shows typical STEM high angle

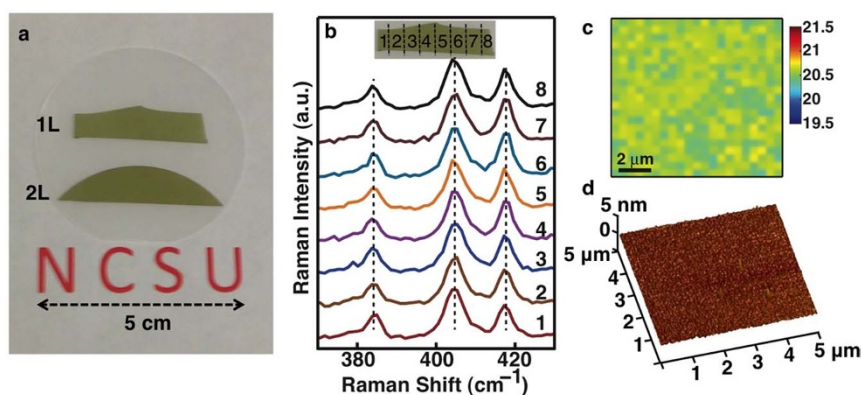


**Figure 2 | Large-area uniformity of the synthesized MoS<sub>2</sub> monolayer and bilayer films.** (a), A picture for as-grown MoS<sub>2</sub> monolayer (1 L) and bilayer (2 L) films, along with a NCSU logo. Underneath the films is a blank sapphire wafer, which is transparent and used as a reference. (b), Raman spectra collected from eight different areas of the MoS<sub>2</sub> monolayer film. The inset schematically illustrates how the eight areas distribute across the substrate. (c), Map of the Raman frequency difference  $\Delta k$  collected from an area of  $10 \mu\text{m} \times 10 \mu\text{m}$  in the MoS<sub>2</sub> monolayer film. All the measured  $\Delta k$  are in the range of  $20.3 - 20.7 \text{ cm}^{-1}$ . Mapping step:  $0.5 \mu\text{m}$ . (d), Perspective view of a typical AFM image collected from the MoS<sub>2</sub> monolayer film. A topview of this AFM image is given as Fig. S7 in the Supplementary Information.

annular dark field (HAADF) image of synthesized monolayers and corresponding fast Fourier transformation (FFT) pattern. The hexagonal atomic arrangement shown in the STEM image and the FFT pattern indicate that the basal plane of the synthesized thin film is (001), i.e. the c-axis of MoS<sub>2</sub> materials perpendicular to the thin film. From the STEM image we can directly measure the lattice constant as  $a = b = 0.32 \text{ nm}$ , consistent with bulk MoS<sub>2</sub> materials. As STEM-HAADF imaging is dependent on the atomic number, we can identify the positions of Mo and S atoms in the monolayer by the difference in image contrast (Mo atoms show much higher contrast than S atoms), as shown in Fig. 3b. Additionally, STEM-HAADF imaging provides a credible way to identify the stacking sequence in MoS<sub>2</sub> bilayers. We can find a substantial difference between the images of MoS<sub>2</sub> monolayer (Fig. 3b) and bilayer (Fig. 3c). This difference indicates an AB stacking sequence in the MoS<sub>2</sub> bilayer, where the Mo atoms of one layer overlap with the position of the sulfur

atoms in the other layer (Fig. S13). The experimental observation matches the modeled image for the AB stacking very well (Fig. 3c).

The synthesized thin films show excellent optical quality that is comparable to exfoliated MoS<sub>2</sub>. Fig. 4a shows the PL spectra collected from exfoliated and synthesized MoS<sub>2</sub> monolayers. Raman peaks of the MoS<sub>2</sub> materials are also included, and the (photoluminescence) PL spectra are normalized to the intensity of corresponding Raman peaks. The normalization is to better correlate the measured PL intensity with the intrinsic luminescence efficiency of the materials<sup>6</sup>. Two peaks can be found in the PL spectra,  $\sim 620 \text{ nm}$  and  $\sim 670 \text{ nm}$ , and can be correlated to the B<sub>1</sub> and A<sub>1</sub> excitons of MoS<sub>2</sub>, respectively<sup>6</sup>. We can find similar PL peaks from both synthesized and exfoliated MoS<sub>2</sub> monolayer. This suggests a comparable optical quality in the synthesized film with the exfoliated MoS<sub>2</sub>. We should note that the synthesized monolayer for the PL measurement was grown on sapphire substrates. For the convenience of comparison with the exfoliated MoS<sub>2</sub>, which were dispersed onto SiO<sub>2</sub>/Si substrates, the synthesized monolayer was transferred to SiO<sub>2</sub>/Si substrates for the PL measurement (see the effect of substrates on PL in Fig. S14). We find that the PL from the MoS<sub>2</sub> monolayer film grown on SiO<sub>2</sub>/Si substrates is much weaker than the films grown on sapphire (Fig. S15), probably due to a poorer crystalline quality in the films grown on SiO<sub>2</sub>/Si substrates than those grown on sapphire as reported previously<sup>25</sup>. Additionally, the PL efficiency of exfoliated MoS<sub>2</sub> has been well known substantially decreasing with the increase in the layer number due to an evolution of the bandgap with the layer number. We can find that the PL efficiency of the synthesized MoS<sub>2</sub> bilayer is indeed substantially smaller than that of synthesized monolayers (Fig. S16). This suggests that the bandgap of the synthesized MoS<sub>2</sub> film bears a similar dependence on the layer number as exfoliated MoS<sub>2</sub>. To illustrate the uniformity of the optical quality, we performed PL mapping over an area of  $20 \mu\text{m} \times 20 \mu\text{m}$  in the synthesized monolayer. The measurement demonstrates a uniform distribution in the PL intensity (Fig. 4a inset), confirming the uniformity as suggested by the Raman measurements shown in the preceding text.

We also evaluated the electrical quality of the synthesized MoS<sub>2</sub> monolayer film. We transferred the thin film grown on sapphire to degenerately doped silicon substrates covered with 280-nm-thick SiO<sub>2</sub>, and fabricated bottom-gate transistors by evaporating 5 nm Ti/200 nm Au electrodes on top of the MoS<sub>2</sub> thin film. We performed electrical measurements at room temperature and in ambient environment using the degenerately doped silicon substrate as a back gate and deposited Au electrodes as the source and drain. Fig. 4b

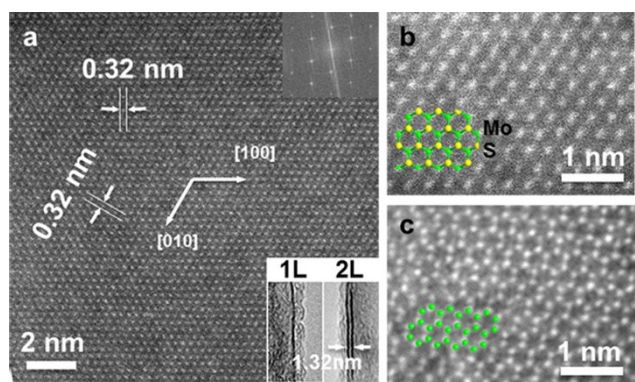


**Figure 3 | Characterization of the crystal structure of synthesized MoS<sub>2</sub> monolayer and bilayer films.** (a), High angle annular dark field (HAADF) image of typical MoS<sub>2</sub> monolayer film. Upper inset is the corresponding FFT pattern, which is not indexed for visual convenience (an indexed version is given in Fig. S12a). Lower inset shows the folded edges of MoS<sub>2</sub> monolayer and bilayer films. The lattice constant and important crystalline directions are given as shown. (b) and (c), HAADF of MoS<sub>2</sub> monolayer and bilayer films. The image of the bilayer film (c) is filtered and the original version is given in Fig. S12b. The insets show modeled crystal structures of MoS<sub>2</sub> monolayer and bilayer films with blue and yellow dots corresponding to Mo and S atoms, respectively. The sulfur atom in the inset of (c) is not given for visual convenience.



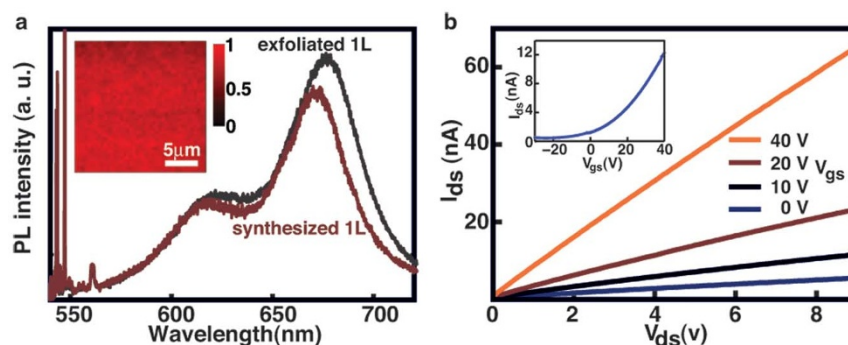


**Figure 4 | Optical and electrical characterizations of the synthesized MoS<sub>2</sub> monolayer films.** (a), Photoluminescence (PL) of the synthesized and exfoliated MoS<sub>2</sub> monolayers. Both were dispersed on SiO<sub>2</sub>/Si substrates. The synthesized monolayer was grown on sapphire substrates and then transferred to SiO<sub>2</sub>/Si substrates for the PL measurement. Using the sample substrate for the PL measurement is for the convenience of comparison. Our experimental results show the PL of MoS<sub>2</sub> films may be affected by the substrate (Fig. S14) (b),  $I_{ds}$ - $V_{ds}$  curve for a field effect transistor (FET) made with the synthesized MoS<sub>2</sub> monolayer with gating voltages  $V_{gs}$  0, 10, 20, 40 V. Inset, transfer characteristic for the FET with a source drain bias  $V_{ds}$  of 2 V.

shows typical output characteristic and transfer characteristic (inset) curves of the device. These results indicate that the device is an n-type channel field effect transistor, consistent with other works on exfoliated MoS<sub>2</sub><sup>7,35,36</sup>. The linear dependence of the current  $I_{ds}$  on the source-drain bias  $V_{ds}$  suggests that the contacts between the MoS<sub>2</sub> thin film and the electrodes are ohmic. This ensures that the observed field effect behavior is from the monolayer MoS<sub>2</sub> channel rather than Schottky barriers at the contact. From the measurements, we can derive the field-effect mobility of charge carriers in the device as  $0.003\text{--}0.03\text{ cm}^2/\text{V}\cdot\text{s}$  by using the expression  $\mu = [dI_{ds}/dV_g] \times [L/(WC_iV_{ds})]$ , where  $L$  and  $W$  is the length and width of the channel, respectively,  $C_i$  is the capacitance of the gating oxide, and  $V_g$  is the bias applied to the back gate. This is reasonably comparable to previous reports on exfoliated monolayers measured in similar conditions (ambient environment, back gating with silicon oxide as the gate oxide)<sup>7,35,36</sup>. We can thus conclude that the synthesized thin film has a reasonably comparable electrical quality with exfoliated MoS<sub>2</sub>.

## Discussion

The observed remarkable uniformity and controllability in the synthesized MoS<sub>2</sub> film strongly suggests that this synthetic process is self-limiting, i.e. the growth may be automatically stopped by some intrinsic factors of the synthetic process. Unlike the self-limiting mechanism for the growth of graphene<sup>37</sup>, which is related with the limited solubility of carbon source in the catalyst of copper, our experimental results suggest that the partial pressure of gaseous MoS<sub>2</sub> species and the interaction of MoS<sub>2</sub> thin films with substrates play key roles in this self-limiting mechanism.

We found in experiments that the layer number of MoS<sub>2</sub> thin films increases with the amount of precursor materials (Table S1, Fig. S17–S18) and the total pressure in the synthetic setup (Fig. S19–S20). We can correlate this to the effect of the two parameters on the partial pressure of gaseous MoS<sub>2</sub> species  $P_{Mo}$ , which we find increasing with the amount of precursor materials and the total pressure (details see Supplementary Information). We believe that the partial pressure  $P_{Mo}$  plays an important role in control of the layer number.

To elucidate the role of  $P_{Mo}$ , we examine the dynamics of the synthetic process, and find that the precipitation reaction  $\text{MoS}_2(g) \rightarrow \text{MoS}_2(s)$  is the rate-determining step, where  $g$  and  $s$  refer to gaseous and solid phases, respectively (details see Supplementary Information). The precipitation reaction is governed by two pressures, the partial pressure of gaseous MoS<sub>2</sub> species ( $P_{Mo}$ ) and the equilibrium vapor pressure (referred as vapor pressure) of MoS<sub>2</sub> in solid phase ( $P_{Mo}^0$ ). The role of  $P_{Mo}$  in control of the layer number is essentially rooted in its role in the thermodynamics and kinetics of the precipitation reaction. The difference between the partial pressure  $P_{Mo}$  and the vapor pressure  $P_{Mo}^0$  provides the thermodynamic

driving force for the precipitation reaction. The partial pressure must be larger than the vapor pressure, i.e.,  $P_{Mo} > P_{Mo}^0$ , to drive the precipitation of gaseous MoS<sub>2</sub> species. Additionally, based on the law of mass reaction, we know that the partial pressure  $P_{Mo}$  also dictates the rate of the precipitation, a larger  $P_{Mo}$  driving a faster precipitation.

The observed dependence of the layer number of MoS<sub>2</sub> films on experimental parameters (the amount of precursor materials and the total pressure) suggests that a larger partial pressure  $P_{Mo}$  tends to give rise to a thicker film (Fig. S21–S22). While a larger  $P_{Mo}$  can cause a larger precipitation rate, we do not think that this kinetic effect would be the major reason for the observed control of layer number. Should the precipitation rate be the major mechanism for the control, it would request a perfect control in timing to stop the precipitation right at the end of the formation of each individual layer, in order to produce the observed uniform MoS<sub>2</sub> films with precisely controlled layer number. This is most unlikely in our synthetic setup. The growth of large-area, highly uniform MoS<sub>2</sub> thin films in our experiments suggests that this precipitation is a self-limiting process, i.e. the precipitation automatically stops at the end of the formation of each individual layer.

We believe that the self-limiting mechanism may lie in a thermodynamic balance between the partial pressure of gaseous MoS<sub>2</sub> species ( $P_{Mo}$ ) and the vapor pressure of MoS<sub>2</sub> thin films ( $P_{Mo}^0$ ) on the substrate. The vapor pressure of MoS<sub>2</sub> thin films could depend on, more specifically, increase with the layer number. As  $P_{Mo}$  is requested larger than  $P_{Mo}^0$  to provide the thermodynamic driving force, the precipitation of gaseous MoS<sub>2</sub> species may be automatically stopped at a specific layer number by control of  $P_{Mo}$ . For instance, an exclusive growth of MoS<sub>2</sub> monolayer could be achieved by controlling the partial pressure  $P_{Mo}$  between the vapor pressures of MoS<sub>2</sub> monolayer ( $P_{Mo,1}^0$ ) and bilayer ( $P_{Mo,2}^0$ ) films as  $P_{Mo,1}^0 < P_{Mo} < P_{Mo,2}^0$ . In this case, the larger vapor pressure of MoS<sub>2</sub> bilayers may automatically prevent the continuous growth once a MoS<sub>2</sub> monolayer film is formed, regardless a continuous supply of MoS<sub>2</sub> species. This indeed matches our observations that the layer number of MoS<sub>2</sub> films shows a step-function dependence on the amount of precursor materials (Table S1). Our hypothesis on the self-limiting mechanism can also be supported by the observed dependence of the layer number on growth temperatures. We find that the layer number of MoS<sub>2</sub> film increases with the temperature of receiving substrates decreasing (Fig. S23). This can be understood that the vapor pressure of MoS<sub>2</sub> thin films  $P_{Mo}^0$  decreases with the temperature, and the same partial pressure  $P_{Mo}$  can drive a deposition of thicker films at lower temperatures.

The dependence of the vapor pressure of MoS<sub>2</sub> thin films on the layer number might be related with the interaction with substrates.



The vapor pressure indicates a capability of atoms escaping from solid phase into gas phase. The interaction of MoS<sub>2</sub> overlayers with substrates could substantially suppress the escaping of MoS<sub>2</sub> atoms, and subsequently cause a decrease in the vapor pressure. This interaction with substrates is expected to relax with the layer number (Fig. S24). As a result, the vapor pressure of MoS<sub>2</sub> thin film may increase with the layer number. Similar suppression effects of substrates on the vapor pressure have been well demonstrated in other materials adsorbed on substrates, for instance, polymers<sup>38</sup>. This dependence of vapor pressures on the layer number of MoS<sub>2</sub> films may provide the possibility of self-limiting growth. We also find in experiments that a precise control of the layer number generally tends to be more difficult for thicker films, for instance, larger than 4, often resulting a mixture of layer numbers. This suggests that the difference between the vapor pressures of MoS<sub>2</sub> films with neighboring layer number ( $P_{\text{Mo},n+1}^{\circ} - P_{\text{Mo},n}^{\circ}$ ,  $n$  refers to the layer number) tends to shrink with an increase in the layer number, which makes the selective growth more difficult.

To further examine the role of the interaction with substrates, we studied the growth on different receiving substrates, the traditional three-dimensional (3D) bonded materials such as sapphire (referred as 3D substrates) and highly ordered pyrolytic graphite (HOPG, from Ted Pella) that has a similar layered structure as MoS<sub>2</sub> (referred as 2D substrates). We grew MoS<sub>2</sub> films on these different substrates under identical experimental conditions (the different substrates were placed side by side in the tube furnace). We can find a substantial difference between the films grown on sapphire and HOPG (Fig. S25). With the same experimental conditions, while the film grown on sapphire substrates is monolayer ( $\Delta k$  20.4 cm<sup>-1</sup>), the one grown on HOPG is bilayer ( $\Delta k$  22.4 cm<sup>-1</sup>). We can exclude out the possibility that the observed difference in the Raman shifts is caused by the difference in substrates (see Supplementary Information). This result confirms that the interaction of MoS<sub>2</sub> films with substrates plays an important role in the self-limiting growth. The strength of the interaction of 2D material overlayer with conventional 3D substrates e.g. sapphire, is well known different from that with 2D substrates (such as HOPG). This difference has been extensively manifested by the van der Waals epitaxial growth of layered materials on 2D substrates<sup>39</sup>. In our experiment, the different interactions of MoS<sub>2</sub> films with sapphire and HOPG might cause different vapor pressures. Therefore, the same partial pressure of MoS<sub>2</sub> can give rise to a growth of thicker MoS<sub>2</sub> film on HOPG.

In conclusion, we demonstrate a new chemical vapor deposition (CVD) approach that can provide capabilities to produce large-area, high quality MoS<sub>2</sub> monolayer and few-layer films with unprecedented uniformity and controllability. While more studies would be necessary to better understand the growth mechanism, our experimental results strongly suggest that this synthetic process is self-limiting dictated by the balance between the equilibrium pressure of MoS<sub>2</sub> thin films and the partial pressure of MoS<sub>2</sub> species in the vapor phase. As a final note, this synthetic approach can be readily scaled up to produce wafer-scale 2D MoS<sub>2</sub> for the development of practical electronic and photonic devices. It is poised to enable 2D MoS<sub>2</sub> as a useful functional material to revolutionize a wide range of fields including information technology, optoelectronics, chemical/biological sensing, and spintronics.

## Methods

MoS<sub>2</sub> thin films were synthesized in a tube furnace as illustrated in Fig. S1. In a typical growth, 1–50 mg of molybdenum chloride (MoCl<sub>5</sub>) powder (99.99%, Sigma-Aldrich) was placed at the center of the furnace and 1 g of sulfur powder (Sigma-Aldrich) were placed at the upstream entry of the furnace. Receiving substrates were placed downstream in a distance of 1–7 centimeters away from the center of the furnace. In typical experiments, the furnace was heated up at a rate of 28°C/min under a flow of Ar gas, held at a setting temperature for 10 min, and then naturally cooled down to room temperature. Typical conditions for high-quality MoS<sub>2</sub> thin film growth include a temperature of 850°C (the temperature for sulfur source is estimated ~ 300°C), a flow rate of 50 sccm, and a pressure around 2 Torr. The layer number of the synthetic

MoS<sub>2</sub> thin film can be controlled by control of the amount of MoCl<sub>5</sub> precursor or the total pressure in the synthetic setup (see Supplementary Information).

The crystal structure of the resulting products were analyzed with transmission electron microscope (TEM, JEOL-2010) and probe aberration-corrected scanning transmission electron microscope (STEM, FEI Titan 80–300 STEM) operated at 200 KV under STEM mode. The as-grown thin film was transferred to TEM grid for the structure characterization. The thickness and surface topology were measured using atomic force microscope (AFM, Veeco Dimension-3000). Raman mapping and photoluminescence (PL) measurements were carried out using Horiba Labram HR800 Raman Microscopy with an excitation wavelength of 532 nm. X-ray photoelectron spectroscopy were performed on SPECS XPS using an Mg K $\alpha$  x ray source. The field-effect transistor device was fabricated by evaporating Ti/Au (5/200 nm) electrodes directly onto top of MoS<sub>2</sub> films transferred to degenerately doped Si substrates with 280 nm thick silicon oxide. A copper grid (100mesh, 30 micron spacing, Ted Pella) was placed on top of the thin film as mask for the electrode fabrication. This gives a relative large channel with a length  $L = 30 \mu\text{m}$  and a width  $W = 230 \mu\text{m}$ . The electrical measurements were performed in ambient conditions using a probe station (Karl Suss PSM6).

- Novoselov, K. S. *et al.* Two-dimensional Gas of Massless Dirac Fermions in Graphene. *Nature* **438**, 197–200 (2005).
- Berger, C. *et al.* Electronic Confinement and Coherence in Patterned Epitaxial Graphene. *Science* **312**, 1191–1196 (2006).
- Huang, X., Qi, X. Y., Boey, F. & Zhang, H. Graphene-Based Composites. *Chem. Soc. Rev.* **41**, 666–686 (2012).
- Huang, X. *et al.* Graphene-Based Materials: Synthesis, Characterization, Properties, and Applications. *Small* **7**, 1876–1902 (2011).
- Mak, K. F., Lee, C., Hone, J., Shan, J. & Heinz, T. F. Atomically Thin MoS<sub>2</sub>: A New Direct-Gap Semiconductor. *Phys. Rev. Lett.* **105**, 136805 (2010).
- Splendiani, A. *et al.* Emerging Photoluminescence in Monolayer MoS<sub>2</sub>. *Nano Lett.* **10**, 1271–1275 (2010).
- Radisavljevic, B., Radenovic, A., Brivio, J., Giacometti, V. & Kis, A. Single-layer MoS<sub>2</sub> Transistors. *Nat Nanotechnol* **6**, 147–150 (2011).
- Wang, H. *et al.* Integrated Circuits Based on Bilayer MoS<sub>2</sub> Transistors. *Nano Lett.* **12**, 4674–4680 (2012).
- Yin, Z. Y. *et al.* Single-Layer MoS<sub>2</sub> Phototransistors. *ACS Nano* **6**, 74–80 (2012).
- Pu, J. *et al.* Highly Flexible MoS<sub>2</sub> Thin-Film Transistors with Ion Gel Dielectrics. *Nano Lett.* **12**, 4013–4017 (2012).
- Kim, S. *et al.* High-mobility and Low-power Thin-film Transistors Based on Multilayer MoS<sub>2</sub> Crystals. *Nat. Comm.* **3**, 1011 (2012).
- Yoon, Y., Ganapathi, K. & Salahuddin, S. How Good Can Monolayer MoS<sub>2</sub> Transistors Be? *Nano Lett.* **11**, 3768–3773 (2011).
- Cao, T. *et al.* Valley-selective Circular Dichroism of Monolayer Molybdenum Disulfide. *Nat. Comm.* **3**, 887 (2012).
- Gunawan, O. *et al.* Valley Susceptibility of an Interacting Two-dimensional Electron System. *Phys. Rev. Lett.* **97**, 186404 (2006).
- Lee, H. S. *et al.* MoS<sub>2</sub> Nanosheet Phototransistors with Thickness-Modulated Optical Energy Gap. *Nano Lett* **12**, 3695–3700 (2012).
- Mak, K. F. *et al.* Tightly Bound Trions in Monolayer MoS<sub>2</sub>. *Nat. Mater.* **12**, 207–211 (2012).
- Mak, K. F., He, K., Shan, J. & Heinz, T. F. Control of Valley Polarization in Monolayer MoS<sub>2</sub> by Optical Helicity. *Nat. Nanotechnol.* **7**, 494–498 (2012).
- Xiao, D., Liu, G. B., Feng, W. X., Xu, X. D. & Yao, W. Coupled Spin and Valley Physics in Monolayers of MoS<sub>2</sub> and Other Group-VI Dichalcogenides. *Phys. Rev. Lett.* **108**, 196802 (2012).
- Zeng, H., Dai, J., Yao, W., Xiao, D. & Cui, X. Valley Polarization in MoS<sub>2</sub> Monolayers by Optical Pumping. *Nat. Nanotechnol.* **7**, 490–493 (2012).
- Chhowalla, M. *et al.* The Chemistry of Ultra-thin Transition Metal Dichalcogenide Nanosheets. *Nat. Chem.* **5** (2013).
- He, Q. *et al.* Fabrication of Flexible MoS<sub>2</sub> Thin-Film Transistor Arrays for Practical Gas-Sensing Applications. *Small* **8**, 2994–2999 (2012).
- Huang, X., Zeng, Z. & Zhang, H. Metal Dichalcogenide Nanosheets: Preparation, Properties and Applications. *Chem. Soc. Rev.* **42**, 1934–1946 (2013).
- Liu, J. *et al.* Preparation of MoS<sub>2</sub>-Polyvinylpyrrolidone Nanocomposites for Flexible Nonvolatile Rewritable Memory Devices with Reduced Graphene Oxide Electrodes. *Small* **8**, 3517–3522 (2012).
- Lee, Y.-H. *et al.* Synthesis of Large-Area MoS<sub>2</sub> Atomic Layers with Chemical Vapor Deposition. *Adv. Mater.* **24**, 2320–2325 (2012).
- Etgar, L. *et al.* High Efficiency Quantum Dot Heterojunction Solar Cell Using Anatase (001) TiO<sub>2</sub> Nanosheets. *Adv. Mater.* **24**, 2202–2206 (2012).
- Zhan, Y., Liu, Z., Najmaei, S., Ajayan, P. M. & J. L. Large-Area Vapor-Phase Growth and Characterization of MoS<sub>2</sub> Atomic Layers on a SiO<sub>2</sub> Substrate. *Small* **8**, 966–971 (2012).
- Lin, Y. C. *et al.* Wafer-scale MoS<sub>2</sub> Thin Layers Prepared by MoO<sub>3</sub> Sulfurization. *Nanoscale* **4**, 6637–6641 (2012).
- Zhang, W. *et al.* Ultrahigh-Gain Phototransistors Based on Graphene-MoS<sub>2</sub> Heterostructures. *arXiv:1302.1230* (2013).
- Shi, Y. *et al.* van der Waals Epitaxy of MoS<sub>2</sub> Layers Using Graphene As Growth Templates. *Nano Lett.* **12**, 2784–2791 (2012).
- Najmaei, S. *et al.* Vapor Phase Growth and Grain Boundary Structure of Molybdenum Disulfide Atomic Layers. *arXiv 1301.2812* (2013).



31. Zande, A. M. v. d. *et al.* Grains and Grain Boundaries in Highly Crystalline Monolayer Molybdenum Disulfide. *arXiv 1301.1985* (2013).
32. Lee, C. *et al.* Anomalous Lattice Vibrations of Single- and Few-Layer MoS<sub>2</sub>. *ACS Nano* **4**, 2695–2700 (2010).
33. Li, H. *et al.* From Bulk to Monolayer MoS<sub>2</sub>: Evolution of Raman Scattering. *Adv. Func. Mater.s* **22**, 1385–1390 (2012).
34. Li, S.-L. *et al.* Quantitative Raman Spectrum and Reliable Thickness Identification for Atomic Layers on Insulating Substrates. *ACS Nano* **6**, 7381–7388 (2012).
35. Novoselov, K. S. *et al.* Two-dimensional Atomic Crystals. *Proc. Natl. Acad. Sci. USA* **102**, 10451–10453 (2005).
36. Li, H. *et al.* Fabrication of Single- and Multilayer MoS<sub>2</sub> Film-Based Field-Effect Transistors for Sensing NO at Room Temperature. *Small* **8**, 63–67 (2012).
37. Li, X. *et al.* Large-Area Synthesis of High-Quality and Uniform Graphene Films on Copper Foils. *Science* **324**, 1312–1314 (2009).
38. Podgornik, P. & Parsegian, V. A. On a Possible Microscopic Mechanism Underlying the Vapor Pressure Paradox. *Biophys. J.* **72**, 942–952 (1997).
39. Ueno, K., Saiki, K., Shimada, T. & Koma, A. Epitaxial Growth of Transition Metal Dichalcogenides on Cleaved Faces of Mica. *J. Vac. Sci. Technol. A* **8**, 68 (1990).

## Acknowledgments

The authors would like to thank Yuntian Zhu for providing access to a Raman spectrometer. L. C. acknowledges a Ralph E. Powe Junior Faculty Enhancement Award for Oak Ridge

Associated Universities. Y. Z. acknowledges the support of Bissell Distinguished Professorship. Part of the work was supported by the Army Research Office (W911NF-11-1-0529).

## Author contributions

Y.Y. and L.C. conceived the experiments. Y.Y. and C.L. performed the synthesis. Y.Y. performed most of the characterizations and device fabrications. Y.L. carried out the STEM characterization. L.S. and Y.Z. performed the Raman and PL mapping. Y.Y. and L.C. analyzed the data. All authors were involved in writing the manuscript.

## Additional information

**Supplementary information** accompanies this paper at <http://www.nature.com/scientificreports>

**Competing financial interests:** The authors declare no competing financial interests.

**License:** This work is licensed under a Creative Commons Attribution-NonCommercial-NoDerivs 3.0 Unported License. To view a copy of this license, visit <http://creativecommons.org/licenses/by-nc-nd/3.0/>

**How to cite this article:** Yu, Y. *et al.* Controlled Scalable Synthesis of Uniform, High-Quality Monolayer and Few-layer MoS<sub>2</sub> Films. *Sci. Rep.* **3**, 1866; DOI:10.1038/srep01866 (2013).